HHS Public Access

Author manuscript

Top Magn Reson Imaging. Author manuscript; available in PMC 2018 December 01.

Published in final edited form as:

Top Magn Reson Imaging. 2017 December ; 26(6): 251–258. doi:10.1097/RMR.0000000000000145.

Quantitative Methods in Abdominal MRI: Perfusion Imaging

Ananth J. Madhuranthakam[1,2], **Qing Yuan**[1], and **Ivan Pedrosa**[1,2]

[1]Department of Radiology. University of Texas Southwestern Medical Center

[2]Advanced Imaging Research Center. University of Texas Southwestern Medical Center

Abstract

Recent improvements in arterial spin labeled (ASL) and vastly under-sampled dynamic contrast enhanced (DCE) MRI acquisitions are providing a new opportunity to explore the routine use of quantitative perfusion imaging for evaluation of a variety of abdominal diseases in clinical practice. In this review, we discuss different approaches for the acquisition and data analysis of ASL and DCE MRI techniques for quantification of tissue perfusion and present various clinical applications of these techniques in both neoplastic and non-neoplastic conditions in the abdomen.

Introduction

Blood flow or perfusion refers to the passage of blood through an organ and represents the main mechanism for the delivery of oxygen and nutrients to healthy and diseased tissue. The level of tissue perfusion (i.e. in ml/100g of tissue/min) varies between different organs in the abdomen and is a reflection of their function and intrinsic ability to maintain constant perfusion despite changes in blood pressure through an auto-regulatory response. Tissue perfusion is proportional to the pressure difference between the arterial and venous sides and inversely proportional to the viscous and geometric resistances (1).

Measurements of blood flow at the tissue level, as opposed to measurements of the intra-vascular blood flow, may provide insights into fundamental pathophysiologic processes. For example, inflammation is intrinsically associated with changes in blood flow, and alterations in microvascular blood flow have been documented in patients with sepsis (2). Similarly, diseases affecting the abdominal viscera are commonly associated with changes in tissue perfusion. Indeed, changes in splanchnic blood flow have been associated with alterations in gastric intramucosal acidosis, multiple organ failure, and increased mortality (3). Additionally, renal microvascular disease has been correlated with the clinical severity of a variety of non-diabetic and diabetic chronic renal diseases (4). Therefore, quantification of organ tissue perfusion may provide a means to assess disease severity objectively.

Furthermore, the formation of new blood vessels, or neoangiogenesis, is a crucial step in the development and growth of neoplasms. Therapies targeted to inhibit the neoangiogenesis pathway have demonstrated unprecedented success in oncologic patients. The assessment of

Corresponding author: Ivan Pedrosa M.D, Ph.D., 2201 Inwood Rd. Suite 201, Dallas, TX 75390, Phone: 214-645 2285, ivan.pedrosa@utsouthwestern.edu.

tumor response to such anti-angiogenic therapies in the metastatic setting is challenging because of the need to evaluate multiple tumor sites and the fact that these drugs inhibit tumor growth but are rarely curative. The ability to measure perfusion in tumors non-invasively may be useful to not only predict the likelihood of response to anti-angiogenic therapy but also to monitor therapeutic response during the course of the disease. In this review, we will discuss the two most commonly used magnetic resonance imaging (MRI)-based approaches to measure tissue perfusion/vascularity in the abdomen, arterial spin labeled (ASL) and dynamic contrast-enhanced (DCE) MRI techniques, and present some common clinical applications for perfusion imaging.

Perfusion imaging: Techniques

a. Arterial Spin Labeled (ASL) MRI

ASL is a non-contrast MRI technique that can measure tissue perfusion (or capillary blood flow) without the administration of exogenous contrast agents. ASL uses highly permeating water as a tracer by magnetically labeling the water protons in the arterial blood and measuring their accumulation in the tissue of interest. Various versions of ASL have been validated in animals using microspheres, while in humans validation has been performed using the gold standard positron emission tomography (PET) with ^{15}O-labeled water in the brain (5). Compared to DCE or dynamic susceptibility contrast (DSC) perfusion measurements, ASL has several advantages. Specifically, ASL does not require the administration of an exogenous agent thus alleviating the concerns of gadolinium accumulation in the brain (6) or nephrogenic systemic fibrosis (NSF) in patients with impaired renal function (7). Unlike DCE/DSC, the contribution of vascular permeability to ASL measured perfusion is negligible (8) enabling absolute perfusion quantification in physiological units (ml/100g/min).

An ASL-MRI acquisition consists of three distinct steps to achieve absolute quantification of tissue perfusion (Fig. 1). First, the acquisition of two images – a control image, where the blood and static tissues are at full magnetization; and a label image, where only the inflowing blood is selectively inverted while the static tissue is maintained at full magnetization. Second, the image reconstruction including the subtraction of labeled images from the control images to generate a perfusion-weighted image (PWI). Third, perfusion quantification by modeling the PWI signal using a proton-density image and acquisition parameters to account for tissue characteristics, to finally generate a quantitative perfusion map in physiological units of ml/100g/min.

i. Acquisition techniques—An ASL acquisition includes spin labeling, during which the inflowing blood is selectively inverted, as well as a post-label delay for the accumulation of the labeled blood in the tissue and the data acquisition. Some versions of the ASL technique remain investigational and have not been approved by the Food and Drug Administration (FDA) for clinical use.

Spin Labeling Approaches: There are two basic approaches with ASL. *Continuous labeling* inverts (or labels) blood as it passes through a narrow labeling plane, while *pulsed ASL* inverts a volume of blood outside the imaging region. *Pulsed labeling*, using a specific

technique called flow alternating inversion recovery (FAIR), has been more widely applied to measure perfusion in abdominal organs (9). With this approach, two images are acquired, one with a selective inversion applied across the imaging slice and the other image acquired with a non-selective inversion (Fig. 2A). The difference between these two images will be proportional to the amount of tissue perfusion in the imaging plane. Typically, the thickness of the slice-selective inversion volume will be set at three to four times the imaging plane thickness to ensure complete inversion of the spins in the imaging plane. The non-selective inversion is applied as a slab-selective inversion, with the slab's thickness approximately ten times the thickness of the slice-selective inversion volume. After a post-label delay (or inversion time), the images are acquired, which when subtracted provides the tissue perfusion. Pulsed labeling techniques including FAIR can be readily implemented on clinical MRI systems. However, pulsed ASL techniques suffer from reduced signal to noise ratio (SNR) compared to continuous ASL, as demonstrated in brain perfusion studies (10).

Due to hardware limitations, continuous ASL was originally feasible on commercially available MR scanners with only short labeling durations (11). The introduction of *pseudo-continuous ASL* (pCASL) marked a significant advancement by replacing the constant radiofrequency (RF) waves used for inversion with pulsed waves, enabling continuous ASL on commercial scanners with longer labeling times, on the order of seconds (12). pCASL was the recommended choice of labeling technique for brain MRI in a recent consensus paper, convened by the members of the perfusion study group of International Society for Magnetic Resonance in Medicine (ISMRM) (13) and is now commercially offered by major MR vendors for brain perfusion measurement. The pCASL approach includes a train of RF and gradient pulses that selectively labels a plane of interest. For example, this can be applied axially across the abdominal aorta for a labeling duration of 1.5–2 seconds. The arterial blood that flows through this labeling plane is inverted via flow driven adiabatic inversion (Fig. 2B). After a post-label delay (e.g. 1.5 seconds), the label image is acquired. The sequence is repeated with the RF pulses phase-cycled during pCASL (control image), such that the blood flow is not inverted, but the magnetization transfer effects in the imaging volume are maintained between the label and the control acquisitions.

Post-Label Delay: This is the time during which the labeled blood is allowed to accumulate in the tissue of interest and will vary depending upon the tissue. For example, a 1.5 second post-label delay has been found to be an optimal time to measure renal cortical perfusion in adult healthy volunteers. This delay time may need to be altered in patients with decreased cardiac output due to prolonged arterial transit time. Additionally, the signal difference in ASL is less than 2% of the fully relaxed background signal. Hence, background suppression (BGS) is essential to improve the robustness of ASL in clinical applications by reducing the standard deviation of the flow measurements due to physiological and instrumental fluctuations (14). This necessity is even greater in body applications due to substantial physiological sources of variation such as cardiac and respiratory motion, bowel peristalsis etc. (15). BGS can be achieved by the application of multiple inversion pulses after labeling. These pulses can reduce background signal to <3% across a wide range of T1 values from 200 to 4200 ms without affecting the perfusion signal. Furthermore, the arrival of blood in the major vasculature after the labeling period has ended may cause signal fluctuations

leading to high intravascular signal, which may confound the tissue perfusion quantification. Inflow saturation (IFS) pulses applied before the data acquisition can reduce these high intravascular signals. Nonlinear optimization schemes have been developed to determine the ideal BGS inversion times and IFS saturation times for a given label duration and post-label delay with both FAIR and pCASL (16).

Data Acquisition: The majority of brain perfusion studies using ASL methods have been performed with a 2D echo-planar imaging (EPI) readout, either using single slice or multi-slice methods, due to the technique's fast acquisition time. Recent studies have proposed volumetric acquisitions with spiral readouts using 3D fast/turbo spin echo (FSE/TSE) sequence for increased SNR (17). However, EPI and spiral readouts have limitations in body applications due to the association between worse off-resonance effects and larger fields of view (18). Cartesian based TSE readout using single-shot (SSFSE/SShTSE/HASTE) or segmented 3D TSE are robust options for perfusion imaging in body applications (19). Alternatively, 2D balanced steady state free precession (bSSFP) acquisitions have also been used with FAIR-based pulsed ASL (9). Regardless of the underlying readout, multiple signal averages are generally acquired to achieve adequate SNR. In the abdomen, acquiring multiple signal averages requires longer acquisition times, and respiratory compensation can be performed using respiratory bellows (20), navigators (21) or a timed-breathing approach, where the subjects are instructed to breath continuously during the labeling period and hold their breath during the acquisition period (15).

ii. Image reconstruction—ASL images are reconstructed by subtracting the label image from the control image to generate the PWI. Since multiple signal averages are typically acquired, the subtracted PWI are averaged together to improve the SNR. Additionally, the SNR of the reconstructed images can be further increased by a factor of $\sqrt{2}$ by using complex subtraction in k-space prior to image reconstruction (15).

iii. Perfusion Quantification—One of the key advantages of ASL acquisition is its ability to quantify absolute perfusion in physiological values of ml/100g/min. The simplified models of pulsed ASL (equation 1) and continuous ASL (equation 2) can be used for perfusion quantification (f) (22).

$$f_{FAIR} = \frac{\Delta M}{M_0} \cdot \frac{6000.\lambda}{2\alpha(TI - T_{sat})} \cdot \frac{1}{\exp(-TI/T_{1,blood})} \quad [1]$$

$$f_{pCASL} = \frac{\Delta M}{M_0} \cdot \frac{6000.\lambda}{2\alpha T_{1,blood}} \cdot \frac{1}{\exp(-PLD/T_{1,blood}) \times (1 - \exp(-\tau/T_{1,blood}))} \quad [2]$$

For FAIR, these variables include: inversion time (TI); first IFS pulse (Tsat); For pCASL, these variables include: label duration (τ); post-label delay (PLD); common variables: blood-tissue partition coefficient (λ=0.9 ml/g); inversion efficiency, α (1 for FAIR, 0.9 for

pCASL without BGS and 0.6 for pCASL with BGS). ΔM is the measured perfusion difference image between label and control and M0 is the measured proton density image using same acquisition parameters without any preparation pulses. For simplified models, the longitudinal relaxation time of blood ($T_{1,blood}$) may be assumed for all tissues, removing the necessity of accurately measuring the T1 of the tissues. The units of ml/g/s are typically converted to the customary physiological literature units of ml/100g/min by multiplying by a factor of 6000. For 2D multi-slice imaging, the values of TI (for FAIR) and τ (for pCASL) in these expressions should be adjusted for each slice to consider the time delay between slice acquisitions.

b. Dynamic contrast enhanced (DCE) imaging

i. Acquisition techniques—DCE MRI is an imaging technique that is based on the paramagnetic effect of gadolinium chelates, which shorten the T1 relaxation times of blood and tissues thereby increasing signal intensity on T1-weighted images by (23). Depending on clinical need and the method used for data analysis, either multi-phasic or high temporal resolution DCE images of the same anatomic volume of interest can be acquired, most commonly using a 3D spoiled gradient echo (SPGR) sequence. For multi-phasic acquisition, baseline images are obtained prior to an intravenous bolus injection of low molecular-weight gadolinium-based contrast agent (GBCA), typically using a power injector at an injection rate of 2–4 mL/s, followed by 20 mL saline flush at the same rate. Using a bolus tracking method, arterial phase, portal venous phase, and equilibrium phase images of the same 3D volume are acquired post-contrast injection. Breath-held multi-phasic images are often obtained with high spatial resolution and fat suppression for superior anatomic delineation and to minimize respiratory motion artifacts. For high temporal resolution DCE-MRI, 3D image sets can be acquired continuously before, during, and after contrast injection for up to 6 minutes. Rapid acquisitions (i.e. with higher temporal resolution) are required to image the signal change induced by the contrast media every few seconds (typically every 4–6 s). However, traditional higher temporal resolution acquisitions require a compromise between anatomic coverage and spatial resolution. Parallel imaging techniques have been widely implemented in DCE-MRI to mitigate this requirement. Other emerging fast imaging techniques such as compressed sensing can also be applied to increase temporal resolution by several fold without sacrificing spatial resolution (24).

In abdominal DCE-MRI, respiratory motion can cause image artifacts and image misregistration. Therefore, DCE images of the abdomen should be acquired with shallow breathing or with sequential breath-holds, with 2 or 3 free breathing respiration cycles between image acquisitions. Recently, radial and spiral acquisitions that undersample high-frequency data while oversampling the low-frequency data at the center of k-space have been implemented and allow for 3D acquisitions of the abdomen with 2–3 second temporal resolutions (24, 25). These sequences are particularly attractive for abdominal imaging because their speed and data acquisition redundancy at the center of k-space make them particularly robust to motion (24). Moreover, the frequent sampling of the center of k-space allows for more accurate determination of contrast dynamics. Some versions of the radial and spiral DCE techniques remain investigational and have not been approved by the Food and Drug Administration (FDA) for clinical use.

Depending on the analysis method used, T1 measurement prior to contrast injection may be needed to quantify contrast agent concentration from the MR signal intensity. The variable flip angle technique (26) using the same 3D SPGR sequence as the DCE scan is typically performed, with the same anatomic coverage and spatial resolution. Baseline T1 maps (T_{10}) can be estimated from these scans in a short scan time, however B1 inhomogeneity can affect the accuracy of these measurements (27).

Tissue enhancement of DCE-MRI can be visually assessed by the interpreting radiologist. Additional qualitative evaluation can be performed by inspecting the shape of the signal intensity time curve (STC), using the following categories: Type I (persistent) refers to a continuous signal intensity increase after contrast injection; Type II (plateau) refers to an initial signal increase followed by a relatively constant signal intensity; Type III (wash-out) refers to an initial contrast uptake peak followed by a signal intensity decrease over time. Even though the qualitative approach is readily accessible, it is inherently subjective, and its nonparametric nature limits its repeatability and usefulness in the diagnostic setting and in clinical trials.

ii. Semi-quantitative analysis (model free)—Semi-quantitative (model-free) analysis of DCE-MRI measures a group of numerical enhancement-related parameters from the STC, which includes peak enhancement, time to peak, wash-in slope, wash-out slope, and area under the curve. Definitions of the most commonly applied parameters can be found in Table 1. Semi-quantitative analysis is less complicated, and all parameters can be calculated directly from image signal intensity without converting those values to GBCA concentration values. However, these parameters depend on the type of image acquisition and injection protocol, which makes the comparison of results obtained at different times, different MRI systems and different sites difficult.

iii. Quantification with Pharmacokinetic models—Quantitative analysis of DCE-MRI using pharmacokinetic modeling has the potential to provide noninvasive measurements and functional characterization of tissue microvasculature. The Tofts model is the most widely used pharmacokinetic model, which includes two tissue compartments representing the intravascular space and the extravascular extracellular space (EES). Depending on blood flow and vessel permeability, low-molecular weight GBCAs can leak out of the capillaries into the EES, and as tissue GBCA concentration increases will diffuse back from the EES to the capillaries until an equilibrium is reached. The original Tofts model (28) assumes that tissue GBCA content is mainly from the EES compartment and that the plasma component is negligible. Contrast agent concentration in tissue (C_t) is given by:

$$C_t(t) = K^{trans} \int_0^t C_p(\tau) \cdot \exp\left(-k_{ep}(t-\tau)\right) \, \mathrm{d}\tau \quad [3]$$

where C_p is contrast agent concentration in the arterial blood plasma. K^{trans} is the transfer constant that characterizes the diffusive transport of contrast agent from intravascular space to EES. The rate constant k_{ep} ($k_{ep} = K^{trans}/v_e$) from ESS to blood plasma, where v_e is the fractional volume of EES, can also be estimated.

The extended Tofts model (29) assumes that tissue concentration of the GBCA represents the sum of contributions from the intravascular and EES compartments, as described by the equation below:

$$C_t(t)=K^{trans}\int_0^t C_p(\tau)\cdot\exp\left(-k_{ep}(t-\tau)\right)\,\mathrm{d}\tau+v_p\cdot C_p(\mathrm{t}) \quad [4]$$

Using this extended Tofts model, the fractional volume of intravascular space, v_p, can also be estimated.

The quantitative pharmacokinetic analysis of DCE data is performed by modeling the GBCA concentration in the various compartments, while the DCE data are measured as MRI signal intensity. Hence, the signal intensities measured by DCE-MRI must be converted into GBCA concentration using known contrast agent relaxivities and the image acquisition parameters. For the T1-weighted SPGR sequence, the MRI signal intensity for each dynamic time point, *t*, is given by (30):

$$S(t)=M_0\cdot\sin(\alpha)\cdot\frac{1-e^{-TR/T_1(t)}}{1-\cos(\alpha)\cdot e^{-TR/T_1(t)}} \quad [5]$$

where the T2* effect is considered negligible due to the short TE used. M_0 is the equilibrium signal intensity that depends on proton density and other scanner scaling factors. α is the flip angle of the acquired pulse sequence. TR is the repetition time. T_1 is the longitudinal relaxation time, which depends on pre-contrast baseline T_1 value, i.e., T_{10}, and the contrast agent concentration (C_t) described by the below equation:

$$\frac{1}{T_1(t)}=\frac{1}{T_{10}}+r_1\cdot C_t(t) \quad [6]$$

where r_1 is the T_1 relaxivity which depends on contrast agent, temperature, and field strength (23). T_{10} can be estimated from the images acquired using the same SPGR sequence with different flip angles, i.e., the variable flip angle method (26). Combining equations [5] and [6], GBCA concentration in tissue can be calculated, with the additional assumption that the concentration is zero prior to contrast injection. GBCA concentration in arterial blood plasma (C_p), i.e. the arterial input function (AIF), can be estimated using the same method. However, it may not be practical to measure the true AIF from the vessel that feeds the tissue of interest due to small vessel size or difficulty localizing the appropriate vessel. If a major artery, such as the aorta, is included in the imaging volume of the dynamic scan, the GBCA concentration from the vessel can be assumed as the AIF in individual patients. Otherwise, population-based AIFs are often used instead of measuring individual AIF (28).

For DCE studies of the liver, a dual-input one-compartmental model is typically used, given the dual blood supply via the hepatic artery and portal vein (25)(31):

$$\frac{dC_L(t)}{dt} = k_{1a} \cdot C_a(t-\tau_a) + k_{1p} \cdot C_p(t-\tau_b) + k_2 \cdot C_L(t) \quad [7]$$

where $C_L(t)$, $C_a(t)$ and $C_p(t)$ represent the contrast concentration in liver, aorta and portal vein, respectively. k_{1a} represents the aortic inflow rate constant, k_{1p} the portal venous inflow rate constant, and k_2 the outflow rate constant. τ_a and τ_b are the transit time for aorta and portal vein, respectively. After converting the DCE signal intensities into contrast concentration and fitting those data to this model, liver perfusion parameters, such as arterial fraction ($AF=k_{1a}/(k_{1a}+k_{1p})$), distribution volume ($DV=(k_{1a}+k_{1p})/k_2$), and mean transit time ($MTT=1/k_2$) can be calculated (Fig. 3).

Clinical Applications

Most clinical applications of perfusion imaging in the abdomen to date have focused on the evaluation of the renal function and cancer. Renal microvascular perfusion is a surrogate marker of renovascular disease (32) and several other medical renal conditions, including diabetes (4). Indeed, previous studies have demonstrated a correlation between renal artery blood flow and the presence of chronic kidney disease (CKD) (33). ASL-derived estimates of cortical perfusion also correlate with CKD stage and the estimated glomerular filtration rate (eGFR) in patients with diabetic nephropathy (34). Similarly, ASL-derived estimates of renal blood flow are statistically different between patients with lupus nephritis and controls (35). ASL is particularly well suited to assess renal transplants because of the common superficial location of renal allografts in the pelvis. This results in little respiratory motion and allows for examination using high-density phased-array surface coils and no GBCA administration. ASL perfusion levels in renal transplants correlate with eGFR and creatinine levels (36). The development of volumetric (3D) pCASL acquisitions (19) provide the opportunity to interrogate renal perfusion in the entire kidney and/or allograft (Fig. 4) and detect regional abnormalities in renal perfusion that may not be detectable with a single measurement of renal artery blood flow.

Both ASL and DCE-MRI techniques can be utilized to estimate the perfusion of renal masses. ASL can detect renal mass perfusion in patients with CKD, potentially obviating the need to administer I.V. contrast (37). Lanzman et al (38) reported the use of ASL to differentiate renal masses with different histologies and found a statistically higher perfusion level in oncocytoma, a benign renal mass, compared with that of primary renal cancer. If this is confirmed in larger series, it could represent a potential use of this technique to recognize these benign tumors non-invasively and avoid unnecessary surgeries; it is virtually impossible to reliably differentiate these entities using conventional MRI techniques. Both ASL perfusion and DCE-derived K^{trans} levels have also been shown to correlate with microvessel density in clear cell renal cell carcinoma (20) and ASL is a surrogate marker of tumor cellularity in these tumors (39).

The increasing role of antiangiogenic therapies in patients with advanced malignancies have highlighted the need to develop prognostic and predictive imaging biomarkers based on the

mechanistic effect of these drugs (i.e. changes in tumor vascularity). Several reports have illustrated the potential to assess tumor response based on tumor perfusion using ASL (40) as well as DCE-MRI (41–43) in a variety of abdominal tumors. Generally, response to antiangiogenic drugs is associated with a decrease in tumor vascularity (Fig. 5) and high pre-treatment baseline tumor vascularity may be predictive of response to these therapies (44, 45). Lastly, novel statistical methods with cluster analysis of quantitative parametric maps derived from DCE-MRI datasets may help predict aggressive histology in renal masses (46) and evaluate heterogeneity in tumor response to anti-angiogenic therapy (47).

Conclusion

The development of novel MRI acquisitions, both without and with exogenous contrast administration, provide a new opportunity to extract direct quantitative measures of tissue perfusion and other vascular-related measures that may provide an objective assessment of disease severity. While ASL-MRI has been extensively studied in humans to measure brain perfusion, these methods for body applications have required a number of innovative technical developments to address specific challenges in body imaging and have only recently become more mature. DCE-MRI acquisitions have been used extensively to quantify tissue vascularity, although traditional approaches suffer from lower temporal resolution and/or sensitivity to motion as well as the potential risks of GBCA administration. The development of new vastly undersampled acquisition schemes have created a new opportunity ultra-fast, motion insensitive strategies that allow more robust DCE acquisitions in routine clinical practice.

Acknowledgments

Funding: NIH R01CA154475 (IP), NIH P50CA196516 (I.P, A.J.M.)

References

1. Jain RK. Determinants of tumor blood flow: a review. Cancer Res. 1988; 48(10):2641–58. [PubMed: 3282647]
2. De Backer D, Creteur J, Preiser JC, Dubois MJ, Vincent JL. Microvascular blood flow is altered in patients with sepsis. Am J Respir Crit Care Med. 2002; 166(1):98–104. [PubMed: 12091178]
3. Takala J. Determinants of splanchnic blood flow. Br J Anaesth. 1996; 77(1):50–8. [PubMed: 8703630]
4. Futrakul N, Futrakul P. Biomarker for early renal microvascular and diabetic kidney diseases. Ren Fail. 2017; 39(1):505–11. [PubMed: 28494191]
5. Ye FQ, Berman KF, Ellmore T, Esposito G, van Horn JD, Yang Y, Duyn J, Smith AM, Frank JA, Weinberger DR, et al. H(2)(15)O PET validation of steady-state arterial spin tagging cerebral blood flow measurements in humans. Magnetic resonance in medicine: official journal of the Society of Magnetic Resonance in Medicine / Society of Magnetic Resonance in Medicine. 2000; 44(3):450–6.
6. McDonald RJ, McDonald JS, Kallmes DF, Jentoft ME, Murray DL, Thielen KR, Williamson EE, Eckel LJ. Intracranial Gadolinium Deposition after Contrast-enhanced MR Imaging. Radiology. 2015:150025.
7. Saleh L, Juneman E, Movahed MR. The use of gadolinium in patients with contrast allergy or renal failure requiring coronary angiography, coronary intervention, or vascular procedure. Catheterization and cardiovascular interventions: official journal of the Society for Cardiac Angiography & Interventions. 2011; 78(5):747–54. [PubMed: 21780275]

8. Wolf RL, Wang J, Wang S, Melhem ER, O'Rourke DM, Judy KD, Detre JA. Grading of CNS neoplasms using continuous arterial spin labeled perfusion MR imaging at 3 Tesla. Journal of magnetic resonance imaging: JMRI. 2005; 22(4):475–82. [PubMed: 16161080]
9. Fenchel M, Martirosian P, Langanke J, Giersch J, Miller S, Stauder NI, Kramer U, Claussen CD, Schick F. Perfusion MR imaging with FAIR true FISP spin labeling in patients with and without renal artery stenosis: initial experience. Radiology. 2006; 238(3):1013–21. [PubMed: 16439565]
10. Wang J, Zhang Y, Wolf RL, Roc AC, Alsop DC, Detre JA. Amplitude-modulated continuous arterial spin-labeling 3.0-T perfusion MR imaging with a single coil: feasibility study. Radiology. 2005; 235(1):218–28. [PubMed: 15716390]
11. Roberts DA, Detre JA, Bolinger L, Insko EK, Lenkinski RE, Pentecost MJ, Leigh JS Jr. Renal perfusion in humans: MR imaging with spin tagging of arterial water. Radiology. 1995; 196(1): 281–6. [PubMed: 7784582]
12. Dai W, Garcia D, de Bazelaire C, Alsop DC. Continuous flow-driven inversion for arterial spin labeling using pulsed radio frequency and gradient fields. Magnetic resonance in medicine: official journal of the Society of Magnetic Resonance in Medicine / Society of Magnetic Resonance in Medicine. 2008; 60(6):1488–97.
13. Alsop DC, Detre JA, Golay X, Gunther M, Hendrikse J, Hernandez-Garcia L, Lu H, MacIntosh BJ, Parkes LM, Smits M, et al. Recommended implementation of arterial spin-labeled perfusion MRI for clinical applications: A consensus of the ISMRM perfusion study group and the European consortium for ASL in dementia. Magn Reson Med. 2015; 73(1):102–16. [PubMed: 24715426]
14. Garcia DM, Duhamel G, Alsop DC. Efficiency of inversion pulses for background suppressed arterial spin labeling. Magnetic resonance in medicine: official journal of the Society of Magnetic Resonance in Medicine / Society of Magnetic Resonance in Medicine. 2005; 54(2):366–72.
15. Robson PM, Madhuranthakam AJ, Dai W, Pedrosa I, Rofsky NM, Alsop DC. Strategies for reducing respiratory motion artifacts in renal perfusion imaging with arterial spin labeling. Magnetic resonance in medicine: official journal of the Society of Magnetic Resonance in Medicine / Society of Magnetic Resonance in Medicine. 2009; 61(6):1374–87.
16. Maleki N, Dai W, Alsop DC. Optimization of background suppression for arterial spin labeling perfusion imaging. Magma. 2012; 25(2):127–33. [PubMed: 22009131]
17. Li Z, Schar M, Wang D, Zwart NR, Madhuranthakam AJ, Karis JP, Pipe JG. Arterial spin labeled perfusion imaging using three-dimensional turbo spin echo with a distributed spiral-in/out trajectory. Magnetic resonance in medicine: official journal of the Society of Magnetic Resonance in Medicine / Society of Magnetic Resonance in Medicine. 2016; 75(1):266–73.
18. Kim DW, Shim WH, Yoon SK, Oh JY, Kim JK, Jung H, Matsuda T, Kim D. Measurement of arterial transit time and renal blood flow using pseudocontinuous ASL MRI with multiple post-labeling delays: Feasibility, reproducibility, and variation. Journal of magnetic resonance imaging: JMRI. 2017
19. Robson PM, Madhuranthakam AJ, Smith MP, Sun MR, Dai W, Rofsky NM, Pedrosa I, Alsop DC. Volumetric Arterial Spin-labeled Perfusion Imaging of the Kidneys with a Three-dimensional Fast Spin Echo Acquisition. Acad Radiol. 2016; 23(2):144–54. [PubMed: 26521186]
20. Zhang Y, Kapur P, Yuan Q, Xi Y, Carvo I, Signoretti S, Dimitrov I, Cadeddu JA, Margulis V, Muradyan N, et al. Tumor Vascularity in Renal Masses: Correlation of Arterial Spin-Labeled and Dynamic Contrast-Enhanced Magnetic Resonance Imaging Assessments. Clin Genitourin Cancer. 2016; 14(1):e25–36. [PubMed: 26422014]
21. Tan H, Koktzoglou I, Prasad PV. Renal perfusion imaging with two-dimensional navigator gated arterial spin labeling. Magnetic resonance in medicine: official journal of the Society of Magnetic Resonance in Medicine / Society of Magnetic Resonance in Medicine. 2014; 71(2):570–9.
22. Buxton RB, Frank LR, Wong EC, Siewert B, Warach S, Edelman RR. A general kinetic model for quantitative perfusion imaging with arterial spin labeling. Magnetic resonance in medicine: official journal of the Society of Magnetic Resonance in Medicine / Society of Magnetic Resonance in Medicine. 1998; 40(3):383–96.
23. Hao D, Ai T, Goerner F, Hu X, Runge VM, Tweedle M. MRI contrast agents: basic chemistry and safety. J Magn Reson Imaging. 2012; 36(5):1060–71. [PubMed: 23090917]

24. Feng L, Grimm R, Block KT, Chandarana H, Kim S, Xu J, Axel L, Sodickson DK, Otazo R. Golden-angle radial sparse parallel MRI: combination of compressed sensing, parallel imaging, and golden-angle radial sampling for fast and flexible dynamic volumetric MRI. Magn Reson Med. 2014; 72(3):707–17. [PubMed: 24142845]
25. Chen Y, Lee GR, Wright KL, Badve C, Nakamoto D, Yu A, Schluchter MD, Griswold MA, Seiberlich N, Gulani V. Free-breathing liver perfusion imaging using 3-dimensional through-time spiral generalized autocalibrating partially parallel acquisition acceleration. Invest Radiol. 2015; 50(6):367–75. [PubMed: 25946703]
26. Wang HZ, Riederer SJ, Lee JN. Optimizing the precision in T1 relaxation estimation using limited flip angles. Magn Reson Med. 1987; 5(5):399–416. [PubMed: 3431401]
27. Brookes JA, Redpath TW, Gilbert FJ, Murray AD, Staff RT. Accuracy of T1 measurement in dynamic contrast-enhanced breast MRI using two- and three-dimensional variable flip angle fast low-angle shot. J Magn Reson Imaging. 1999; 9(2):163–71. [PubMed: 10077009]
28. Tofts PS, Kermode AG. Measurement of the blood-brain barrier permeability and leakage space using dynamic MR imaging. 1. Fundamental concepts. Magn Reson Med. 1991; 17(2):357–67. [PubMed: 2062210]
29. Tofts PS, Brix G, Buckley DL, Evelhoch JL, Henderson E, Knopp MV, Larsson HB, Lee TY, Mayr NA, Parker GJ, et al. Estimating kinetic parameters from dynamic contrast-enhanced T(1)-weighted MRI of a diffusable tracer: standardized quantities and symbols. J Magn Reson Imaging. 1999; 10(3):223–32. [PubMed: 10508281]
30. Fram EK, Herfkens RJ, Johnson GA, Glover GH, Karis JP, Shimakawa A, Perkins TG, Pelc NJ. Rapid calculation of T1 using variable flip angle gradient refocused imaging. Magn Reson Imaging. 1987; 5(3):201–8. [PubMed: 3626789]
31. Materne R, Smith AM, Peeters F, Dehoux JP, Keyeux A, Horsmans Y, Van Beers BE. Assessment of hepatic perfusion parameters with dynamic MRI. Magn Reson Med. 2002; 47(1):135–42. [PubMed: 11754452]
32. Winter JD, St Lawrence KS, Cheng HL. Quantification of renal perfusion: comparison of arterial spin labeling and dynamic contrast-enhanced MRI. J Magn Reson Imaging. 2011; 34(3):608–15. [PubMed: 21761490]
33. Khatir DS, Pedersen M, Jespersen B, Buus NH. Evaluation of Renal Blood Flow and Oxygenation in CKD Using Magnetic Resonance Imaging. Am J Kidney Dis. 2015; 66(3):402–11. [PubMed: 25618188]
34. Mora-Gutierrez JM, Garcia-Fernandez N, Slon Roblero MF, Paramo JA, Escalada FJ, Wang DJ, Benito A, Fernandez-Seara MA. Arterial spin labeling MRI is able to detect early hemodynamic changes in diabetic nephropathy. J Magn Reson Imaging. 2017
35. Rapacchi S, Smith RX, Wang Y, Yan L, Sigalov V, Krasileva KE, Karpouzas G, Plotnik A, Sayre J, Hernandez E, et al. Towards the identification of multi-parametric quantitative MRI biomarkers in lupus nephritis. Magn Reson Imaging. 2015; 33(9):1066–74. [PubMed: 26119419]
36. Heusch P, Wittsack HJ, Heusner T, Buchbender C, Quang MN, Martirosian P, Bilk P, Kropil P, Blondin D, Antoch G, et al. Correlation of biexponential diffusion parameters with arterial spin-labeling perfusion MRI: results in transplanted kidneys. Invest Radiol. 2013; 48(3):140–4. [PubMed: 23249648]
37. Pedrosa I, Rafatzand K, Robson P, Wagner AA, Atkins MB, Rofsky NM, Alsop DC. Arterial spin labeling MR imaging for characterisation of renal masses in patients with impaired renal function: initial experience. Eur Radiol. 2012; 22(2):484–92. [PubMed: 21877173]
38. Lanzman RS, Robson PM, Sun MR, Patel AD, Mentore K, Wagner AA, Genega EM, Rofsky NM, Alsop DC, Pedrosa I. Arterial spin-labeling MR imaging of renal masses: correlation with histopathologic findings. Radiology. 2012; 265(3):799–808. [PubMed: 23047841]
39. Yuan Q, Kapur P, Zhang Y, Xi Y, Carvo I, Signoretti S, Dimitrov IE, Cadeddu JA, Margulis V, Brugarolas J, et al. Intratumor Heterogeneity of Perfusion and Diffusion in Clear-Cell Renal Cell Carcinoma: Correlation With Tumor Cellularity. Clin Genitourin Cancer. 2016; 14(6):e585–e94. [PubMed: 27209349]
40. de Bazelaire C, Alsop DC, George D, Pedrosa I, Wang Y, Michaelson MD, Rofsky NM. Magnetic resonance imaging-measured blood flow change after antiangiogenic therapy with PTK787/ZK

222584 correlates with clinical outcome in metastatic renal cell carcinoma. Clin Cancer Res. 2008; 14(17):5548–54. [PubMed: 18765547]

41. Rosen MA, Schnall MD. Dynamic contrast-enhanced magnetic resonance imaging for assessing tumor vascularity and vascular effects of targeted therapies in renal cell carcinoma. Clin Cancer Res. 2007; 13(2 Pt 2):770s–6s. [PubMed: 17255308]
42. Consolino L, Longo DL, Sciortino M, Dastru W, Cabodi S, Giovenzana GB, Aime S. Assessing tumor vascularization as a potential biomarker of imatinib resistance in gastrointestinal stromal tumors by dynamic contrast-enhanced magnetic resonance imaging. Gastric Cancer. 2016
43. Duffy AG, Ulahannan SV, Cao L, Rahma OE, Makarova-Rusher OV, Kleiner DE, Fioravanti S, Walker M, Carey S, Yu Y, et al. A phase II study of TRC105 in patients with hepatocellular carcinoma who have progressed on sorafenib. United European Gastroenterol J. 2015; 3(5):453–61.
44. Flaherty KT, Rosen MA, Heitjan DF, Gallagher ML, Schwartz B, Schnall MD, O'Dwyer PJ. Pilot study of DCE-MRI to predict progression-free survival with sorafenib therapy in renal cell carcinoma. Cancer Biol Ther. 2008; 7(4):496–501. [PubMed: 18219225]
45. Schor-Bardach R, Alsop DC, Pedrosa I, Solazzo SA, Wang X, Marquis RP, Atkins MB, Regan M, Signoretti S, Lenkinski RE, et al. Does arterial spin-labeling MR imaging-measured tumor perfusion correlate with renal cell cancer response to antiangiogenic therapy in a mouse model? Radiology. 2009; 251(3):731–42. [PubMed: 19474376]
46. Xi Y, Yuan Q, Zhang Y, Madhuranthakam AJ, Fulkerson M, Margulis V, Brugarolas J, Kapur P, Cadeddu JA, Pedrosa I. Statistical Clustering of Parametric Maps from Dynamic Contrast Enhanced MRI and an Associated Decision Tree Model for Non-Invasive Tumor Grading of T1b Solid Clear Cell Renal Cell Carcinoma. Eur Radiol. in press.
47. Longo DL, Dastru W, Consolino L, Espak M, Arigoni M, Cavallo F, Aime S. Cluster analysis of quantitative parametric maps from DCE-MRI: application in evaluating heterogeneity of tumor response to antiangiogenic treatment. Magn Reson Imaging. 2015; 33(6):725–36. [PubMed: 25839393]

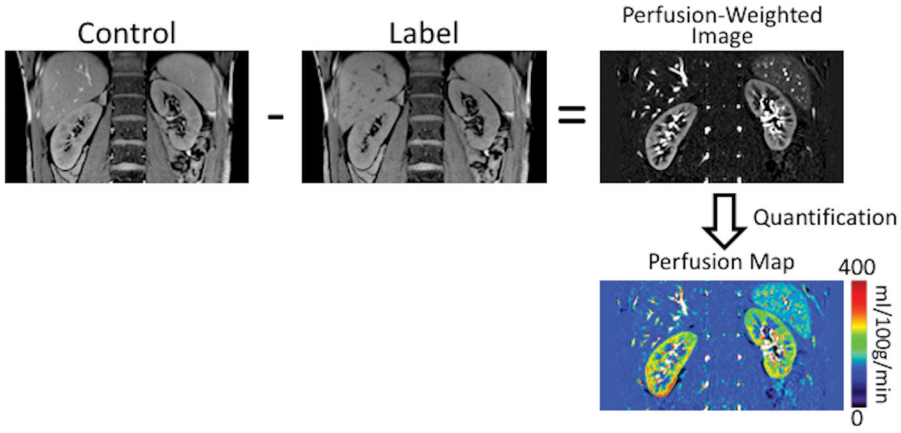

Figure 1.

Schematic of an ASL acquisition applied to estimate kidney perfusion. The acquisition includes a control image, where the magnetization is maintained at an equilibrium, and a label image, where the inflowing blood is selectively inverted. The subtraction of the label image from the control image generates the perfusion-weighted image. Using a separately acquired proton-density image and the perfusion quantification model, absolute perfusion maps in physiological values of ml/100g/min can be generated.

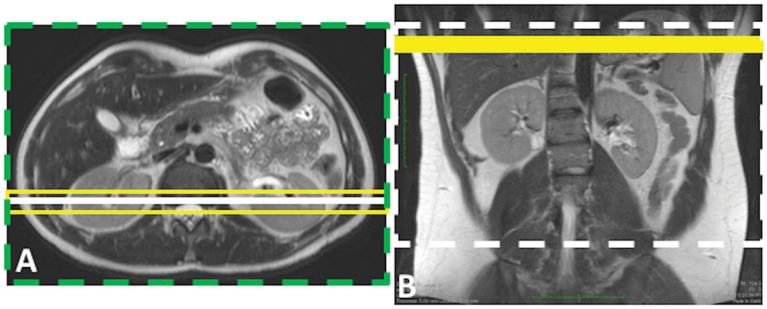

Figure 2.

Schematic of two ASL labeling schemes, including pulsed ASL using FAIR (A) and continuous ASL using pCASL (B). In both schemes, a coronal image is acquired, shown by a solid white line on the axial image (A) and the dashed white line on the coronal image (B). FAIR images are acquired using a slice-selective inversion (yellow box, A) and a non-selective inversion (green dashed box, A). Yellow solid box (B) shows the pCASL labeling plane.

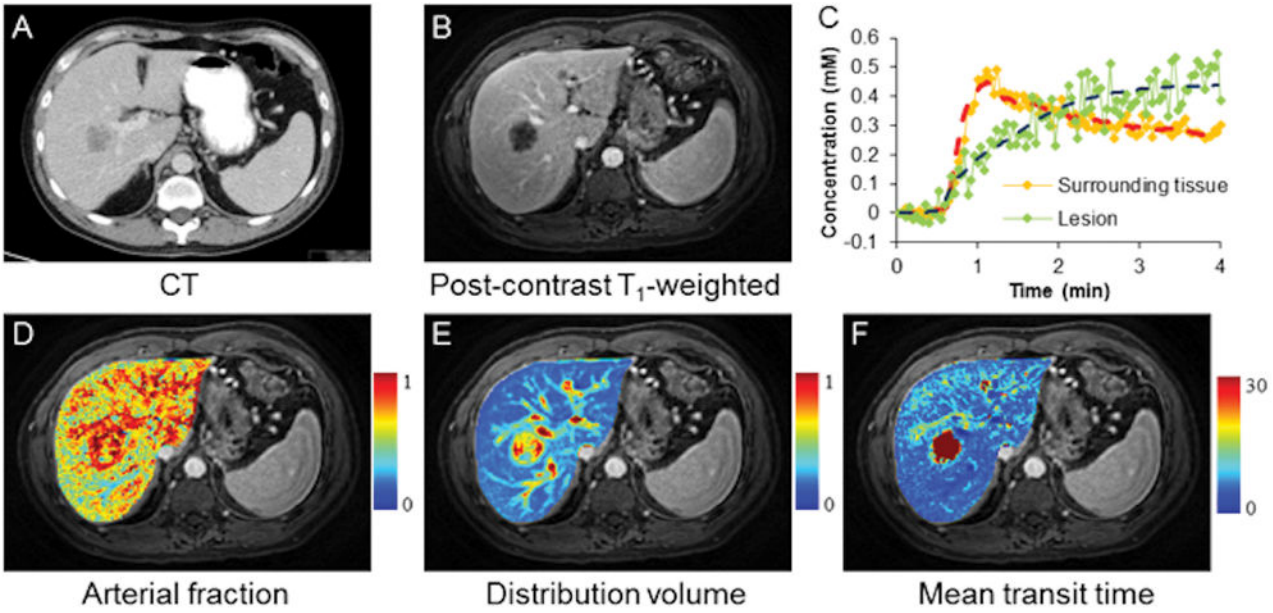

Figure 3.

Free-breathing liver perfusion imaging using through-time spiral generalized auto-calibrating partially parallel acquisition acceleration (GRAPPA). Representative images acquired from a patient with metastatic lung adenocarcinoma. One hundred volumes were acquired continuously over a period of approximately 4 minutes with a spatial resolution of $1.9\times1.9\times3\ mm^3$. (A) Computed tomography image; (B) Representative free-breathing liver DCE image acquired using through-time spiral GRAPPA; (C) Single-voxel GBCA concentration curves from both lesion and surrounding tissue. Fitted data using a dual-input single-compartment model were also plotted. Corresponding perfusion maps including arterial fraction (%), distribution volume (%) and mean transit time (sec) are shown in D–F (Courtesy of Drs. Yong Chen and Vikas Gulani).

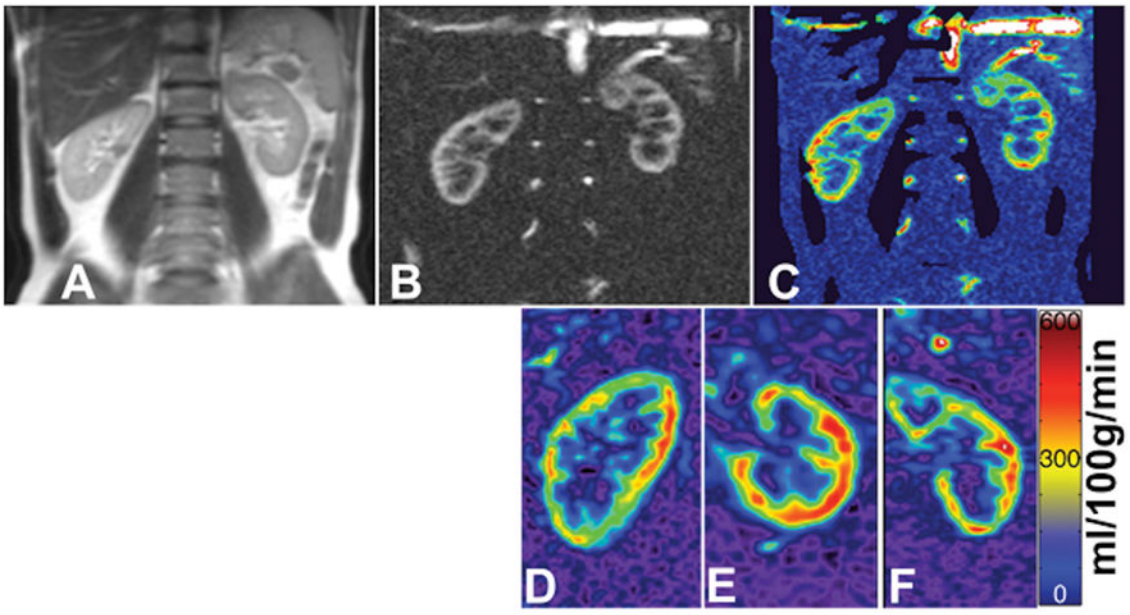

Figure 4.

Perfusion images obtained from the kidneys of a healthy volunteer acquired using pCASL. Shown are a T2-weighted image (a), PWI using 2D pCASL (b), 2D quantitative perfusion map (c), and 3D quantitative perfusion maps (d–f). 3D images were acquired in the sagittal (d) orientation and reformatted to axial (e) and coronal (f) planes. Images were acquired with pCASL labeling using background suppression and Cartesian acquisition with a 2D SShTSE (b,c) and 3D TSE (d–f).

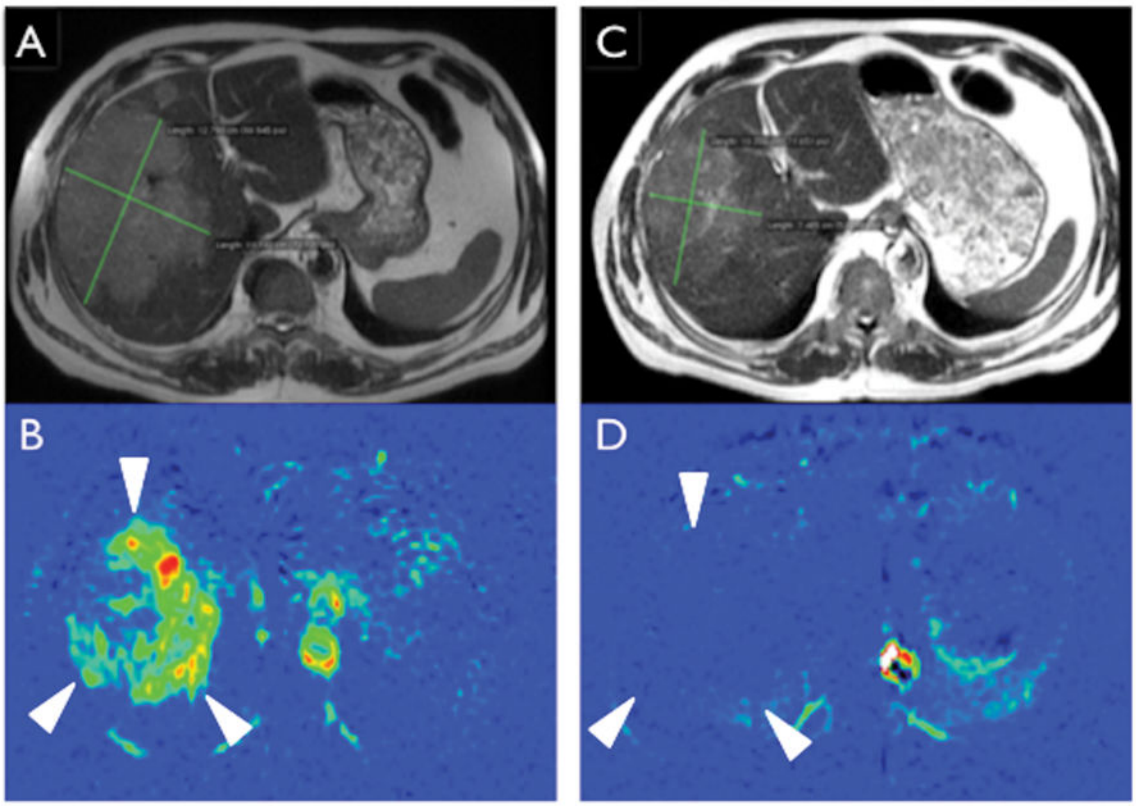

Figure 5.

ASL assessment of response to antiangiogenic therapy in metastatic clear cell renal cell carcinoma. (A) Axial single shot fast spin echo image of the upper abdomen demonstrating a large metastatic lesion in the liver measuring 12.8 × 10.1 cm. (B) Concurrent axial pCASL acquisition demonstrates high perfusion level in the liver mass (arrowheads). (C) After two cycles of treatment with pazopanib, the mass decreased in size to 10.3 × 7.4 cm, just reaching the threshold for partial response (20% decrease). However, pCASL demonstrates nearly complete absence of tumor perfusion, more clearly illustrating the anti-angiogenic therapeutic effect.

Table 1

Semi-quantitative Parameters

	Description
Peak enhancement	The difference between the maximum signal intensity and baseline signal intensity. A ratio of the maximum signal and baseline signal intensities, or the relative signal intensity change between the maximum and baseline signal intensities can be used.
Time to peak	The time from baseline to the peak of the Signal Intensity Time Curve (STC)
Wash-in slope	The slope of the uptake of the STC from the baseline to the peak of the STC
Wash-out slope	The slope of the STC from the maximum signal intensity to the end of the STC
Area under the curve	The area under the STC. The area calculated from the initial uptake portion of the STC for a time point is most commonly used, such as iAUC60 refers to the area under the initial uptake curve for the first 60 seconds.